Chemical Physics Letters 826 (2023) 140682

Contents lists available at ScienceDirect

Chemical Physics Letters

journal homepage: www.elsevier.com/locate/cplett

Research paper

Analysis of entropy generation of a chemically reactive nanofluid by using Joule heating effect for the Blasius flow on a curved surface

M. Naveed

[a] Department of Mathematics, Division of Science and Technology, University of Education, Lahore 54770, Pakistan

ARTICLE INFO

Keywords:
Blasius flow
Buongiorno model
Curved surface
Joule heating
Entropy generation
Numerical solutions

ABSTRACT

This aim of the current study is to discuss the flow, heat and mass transfer in the Blasius flow of a nanofluid towards a curved surface. The energy equation is formulated by considering the Joule heating effect along with heat generation. For nanofluid model we have considered the Buongiorno model. In addition, the influence of both homogenous and heterogeneous chemical reaction is also incorporated in the nanoparticle concentration equation. For optimization of energy we have used entropy generation method (EGM). For the mathematical development of the flow problem we have used the curvilinear coordinate system. The developed partial differential equations are reduced into ordinary differential equation by employing suitable similarity transformations and then solved numerically by shooting method along with Runge-Kutta integrating scheme. The validity of the obtained numerical results is also verified by Keller-box method. The impacts of multifarious parameter particularly, magnetic parameter, radius of curvature, thermophoresis parameter, Brownian motion parameter, heat source parameter, Brinkman number and homogenous-heterogeneous parameters on velocity, temperature, concentration, entropy generation and Bejan number are given through graphs and are discussed in detail. Furthermore, skin friction coefficient, Nusselt number and Schmidt number are discussed for various involved parameters in form of tables.

1. Introduction

Owing to extensive functional applications in numerous industrial and engineering procedures many researchers have kept an eye on the investigation of steady boundary layer flow and convective heat transfer analysis. Such procedures include drawing of plastic film, crystal growing, paper production, metal spinning, cooling of continuous filaments or strips, glass blowing, extrusion pf plastic and rubber sheet. The standard of the conclusive product is strongly reliant on the rate of heat transfer and skin friction coefficient as discussed by Karwe and Jaluria [1]. The boundary layer flow due to uniform free stream velocity on a static surface was introduced by Blasius [2] and hence named after the scientist. Pantokratoras and Fang [3] investigated a study to analyze the heat transfer analysis towards the Blasius flow by including the nonlinear thermal radiation. Naveed et al. [4] examined the nonlinear radiative heat transfer in the Blasius and Skiadas flow over a curved surface. Devi and Suriyakumar [5] analyzed the impact of magnetic field to the Blasius/Sakiadis flow of nanofluid. For more extensive detail about the different aspects of heat transfer for Blasius flow, the interested researchers must read the articles [6–10] and reference therein.

Over the past few decades, many researchers have focused on nanofluid technology to control the heat and mass transport mechanism in different energy devices. The effective use of nanoparticles enhances the basic thermal characteristics of heat transfer and to regulate the cooling techniques. These nanometer sized particles show peculiarities among the physical and chemical demeanor. They demonstrate smoothness in their flow without clogging in micro-channel. Choi [11] comes up with the fundamental concept of nanofluid. Nanofluid depicts great diversity in terms of physical application in heating and boiling processes of energy, electronic devices, thermal absorption, nuclear reactions and lots of other. The characteristics of transport mechanism in nanofluids can be investigated by a nanofluid model developed by Buongiorno [12]. He created a mathematical model for heat and mass transfer in nanofluids which consists of thermophoresis and Brownian diffusion. The impacts of Brownian diffusion and thermophoresis parameter on the Blasius flow towards a curved surface was observed by Naveed et al. [13]. Ganesh et al. [14] analyzed the heat transfer analysis with viscous dissipation impact for the Blasius and Sakiadis slip flow of nanofluid with different size and shapes of nanoparticles. Kumar et al. [15] examined the three-dimensional Blasius/Sakiadis flow of Casson

E-mail address: muhammad.naveed@ue.edu.pk.

https://doi.org/10.1016/j.cplett.2023.140682
Received 29 March 2023; Received in revised form 7 June 2023; Accepted 14 June 2023
Available online 19 June 2023

nanofluid embedded in a Darcy-Forchheimer space. For more detail, regarding the flow of nanofluid the readers are referred to the articles [16–26] and reference therein.

Examination of flow behavior in presence of chemical reactions has gained much attention by significant number of researchers because such types of flow plays an important role in groves of fruit trees, chemical and food processing, hydrometallurgical industry, air and water pollution and many more. The molecular disintegration of species cannot be ignored in accordance with the chemical reactions during such process. Biological processes, combustion and catalysis are a few examples of chemically reactive structures that contains both homogeneous and heterogeneous chemical reactions. These chemical reactions interact with one another in a very complex way. Sajid et al. [27] investigated the properties of homogenous-heterogeneous chemical reactions on magnetic nanoparticles for the Blasius flow. Abbas et al. [28] has scrutinized the impact of equally diffusive chemical reaction in Casson nanoliquid with thermal radiation across a curved oscillating surface. Opanuga et al. [29] examined the impacts of magnetic field along with chemical reaction in the viscous fluid for the Blasius/Sakiadis flow. Ali et al. [30] investigated the bio-convective MHD Blasius flow with chemical reaction. The readers are directed to the publications [31–35] and reference therein for additional information for different fluids with homogenous and heterogeneous chemical reactions over various geometries.

Entropy optimization is considered to be very beneficial and received significant amount of attention by researchers in numerous energy involving system which consist of cooling of new electronic system, solar power collector, thermal energy and geothermal energy system. The study of entropy generation provides a convenient technique to estimate the irreversibility in any thermal procedures. Irreversible procedures consist of flow of fluid due to friction between the viscous fluid, diffusion, resistance flow, chemical reaction, thermal radiation and Joule heating etc. To improve the performance of the thermal system we can control the entropy generation rate. Afridi and Qasim [36] discussed the entropy generation for the Blasius flow with viscous dissipation and nonlinear thermal radiation. Abbas et al. [37] examined the entropy generation with thermal radiation for the hydromagnetic flow of viscous fluid via a vertical plate. Khan et al. [38] studied the estimate the entropy generation for the MHD flow of viscous fluid on a curved stretching surface in presence of cubic autocatalysis chemical reactions. Recently, Khan et al. [39] discussed the entropy generation for the Blasius flow over a flat surface by incorporating variable viscosity and thermal conductivity. Readers interested in learning more about the examination of entropy generation for different fluid models and their physical effects are referred to the papers [40–44] and reference therein.

The main focus of the current examination is to examine the heat and mass transfer investigation in the nanofluid for the Blasius flow on a curved surface with applied magnetic field. Furthermore, optimization of energy is also carried out by considering entropy generation method. Energy equation is formulated by considering Joule heating effect and heat generation. Moreover, the nanoparticle concentration equation includes the effects of heterogeneous and homogeneous chemical reactions. The obtained set of coupled differential equations are than solve numerically by shooting technique. The numerical findings by shooting process are also validated by a finite difference method known as Keller box method. The influence of the physical pertinent parameters on flow, concentration, heat and entropy generation are given via graphs and table and are examined thoroughly.

2. Mathematical formulation

2.1. Flow analysis

Consider two dimensional and an incompressible flow of nanofluid on a curved surface which is bend in a shape of semi-circle of radius R_0. Fig. 1 shows a schematic flow geometry. Let M_0 be the strength of the magnetic field which is applied perpendicular to the flow direction (i.e. in the r direction). By these assumptions, the continuity and momentum equations are given as [27]

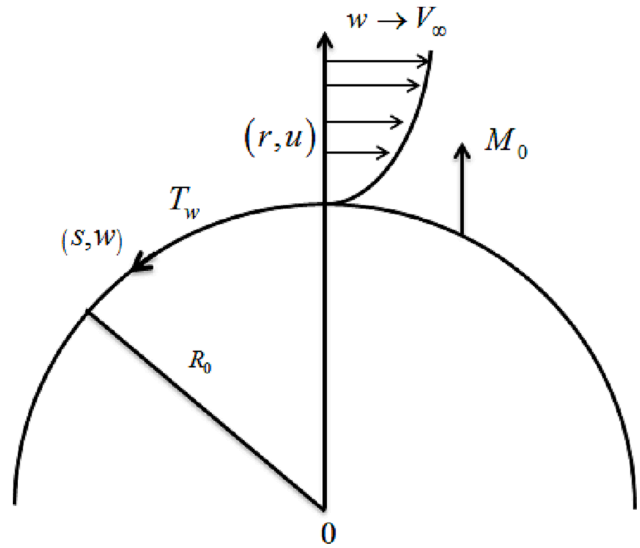

Fig. 1. Geometry of the problem.

$$\frac{\partial}{\partial r}[u(r+R_0)] + R_0\frac{\partial w}{\partial s} = 0, \tag{1}$$

$$\frac{w^2}{r+R_0} = \frac{1}{\rho_f}\frac{\partial p}{\partial r}, \tag{2}$$

$$u\frac{\partial w}{\partial r} + \frac{R_0 w}{r+R_0}\frac{\partial w}{\partial s} + \frac{uw}{r+R} = -\frac{1}{\rho_f}\frac{R_0}{(r+R_0)}\frac{\partial p}{\partial s} + \nu_f\left[\frac{\partial^2 w}{\partial r^2} + \frac{1}{(r+R_0)}\frac{\partial w}{\partial r} - \frac{w}{(r+R_0)^2}\right] - \frac{\sigma M_o^2(w-V_\infty)}{\rho_f}. \tag{3}$$

Subject to the boundary conditions for the velocity field as

$$\begin{aligned} w = 0 = u \quad & \text{at } r = 0, \\ w \to V_\infty \quad & \text{at } r \to \infty. \end{aligned} \tag{4}$$

Here w and u are the velocity components in s and r directions, ν_f is the kinematics viscosity, p is the pressure, ρ_f is the density of the fluid and V_∞ be a constant free stream velocity.

For Blasius flow, we will introduce the following similarity variables as [13]:

$$\begin{aligned} & w = V_\infty f'(\eta), \quad u = \frac{R_0}{2(r+R_0)}\sqrt{\frac{V_\infty \nu_f}{s}}[\eta f'(\eta) - f(\eta)], \\ & p = \rho_f V_\infty^2 P_1(\eta), \quad \eta = r\sqrt{\frac{V_\infty}{s\nu_f}}. \end{aligned} \tag{5}$$

In above equation, f and η are the dimensionless stream function and similarity variable respectively, with $Re_s = sV_\infty/\nu_f$ is the local Reynolds number.

With the help of Eq. (5), the continuity equation given in Eq. (1) is identically hold, and remaining Eqs. (2)–(5) yields

$$\frac{\partial P_1}{\partial \eta} = \frac{f'^2}{\eta + Rc}, \tag{6}$$

$$f''' + \frac{Rc}{2(\eta+Rc)}ff'' - \frac{Rc}{2(\eta+Rc)^2}\left(\eta f'^2 - ff'\right) + \frac{\eta Rc}{2(\eta+Rc)}\frac{\partial P_1}{\partial \eta} - \frac{f'}{(\eta+Rc)^2} + \frac{f''}{\eta+Rc} + M_1(f'-1) = 0, \tag{7}$$

$$f(0) = 0 = f'(0),\quad f'(\infty) = 1. \tag{8}$$

Here $Rc = R_0 V_\infty/\nu_f$ and $M_1 = \sigma s M_0^2/V_\infty \rho_f$ are the dimensionless radius of curvature and magnetic parameter respectively.

Eliminating the pressure term from Eqs. (6) and (7), one can obtain

$$f''' + \frac{f''}{(\eta+Rc)} - \frac{f'}{(\eta+Rc)^2} + \frac{Rcf}{2(\eta+Rc)}\left(f'' + \frac{f'}{(\eta+Rc)}\right) - M_1(f'-1) = 0. \tag{9}$$

It is important to mentioning here that by setting $M_1 = 0$ and $R_c \to \infty$, Eq. (9) transform to classical momentum equation for Blasius flow.

2.2. Transport equations

For the transport phenomenon (heat and mass transfer) the energy equation is modelled by considering the Joule heating effects along with the heat generation. Furthermore, in concentration equation we have considered homogeneous and heterogeneous isothermal chemical reactions which are given as

$$X_1 + 2Y_1 \to 3Y_1 \ \text{rate} = k_\lambda C_\alpha C_\beta^2,\quad X_1 \to Y_1 \ \text{rate} = k_1 C_\alpha. \tag{10}$$

In above equations C_α is the concentration of the species X_1 and C_β is the concentration for species Y_1 with k_λ and k_1 indicates the constant rate. Also let the temperature at the surface be T_w and T_∞ be the free stream temperature with $T_w > T_\infty$.

By considering these assumptions the energy and concentration equations are given by [38]

$$u\frac{\partial T}{\partial r} + \frac{wR_0}{r+R_0}\frac{\partial T}{\partial s} = \frac{k_\gamma}{\rho_f c_p}\left[\frac{\partial^2 T}{\partial r^2} + \frac{1}{r+R_0}\frac{\partial T}{\partial r}\right] + \frac{\tau}{\rho_f c_p}\left\{D_\beta\left(\frac{\partial C_\beta}{\partial r}\frac{\partial T}{\partial r}\right) + \frac{D_T}{T_\infty}\left(\frac{\partial T}{\partial r}\right)^2\right\} + \frac{\sigma M_0^2(w-V_\infty)}{\rho_f} + \frac{B(T-T_\infty)}{\rho_f c_p}, \tag{11}$$

$$u\frac{\partial C_\alpha}{\partial r} + \frac{wR_0}{r+R_0}\frac{\partial C_\alpha}{\partial s} = D_\alpha\left[\frac{\partial^2 C_\alpha}{\partial r^2} + \frac{\partial C_\alpha}{\partial r}\frac{1}{(r+R_0)}\right] + \frac{D_T}{T_\infty}\left[\frac{\partial^2 T}{\partial r^2} + \frac{1}{(r+R_0)}\frac{\partial T}{\partial r}\right] - k_\lambda C_\alpha C_\beta^2, \tag{12}$$

$$u\frac{\partial C_\beta}{\partial r} + \frac{wR_0}{r+R_0}\frac{\partial C_\beta}{\partial s} = D_\beta\left[\frac{\partial^2 C_\beta}{\partial r^2} + \frac{1}{(r+R_0)}\frac{\partial C_\beta}{\partial r}\right] + \frac{D_T}{T_\infty}\left[\frac{\partial^2 T}{\partial r^2} + \frac{1}{(r+R_0)}\frac{\partial T}{\partial r}\right] + k_\lambda C_\alpha C_\beta^2. \tag{13}$$

Where k_γ represents the thermal conductivity, $\tau = (\rho c)_p/(\rho c)_f$ is used to show the ratio of heat capacity of the nanoparticles to the heat capacity of the fluid, D_T represents the thermophoretic diffusion, B is the temperature dependent constant, D_α and D_β represents the diffusion coefficients, c_p is the specific heat at constant pressure and σ be the electrical conductivity.

The boundary conditions correspondence to temperature and concentration field are

$$T = T_w,\ D_\alpha\frac{\partial C_\alpha}{\partial r} = k_1 C_\alpha,\ D_\beta\frac{\partial C_\beta}{\partial r} = -k_1 C_\alpha,\quad \text{at } r = 0,$$
$$T \to T_\infty,\quad C_\alpha \to C_\infty,\ C_\beta \to 0,\quad \text{at } r \to \infty. \tag{14}$$

Eqs. (11)–(14) are reduced into ordinary differential equation by means of similarity transformation as given in Eq. (5) along with

$$\theta(\eta) = \frac{T-T_\infty}{T_w-T_\infty},\quad g(\eta) = \frac{C_\alpha}{C_\infty},\quad \varphi(\eta) = \frac{C_\beta}{C_\infty}. \tag{15}$$

The transformed energy and concentration equations along with boundary condition are given as follows:

$$\left(\theta'' + \frac{\theta'}{\eta+Rc}\right) + \frac{RcPrf\theta'}{2(\eta+Rc)} + Nb_1 Pr\theta'\varphi' + Pr\left(Nt_1\theta'^2 + EcM_1(f'-1) + \alpha_1\theta\right) = 0, \tag{16}$$

$$\left[g'' + \frac{g'}{(\eta+Rc)}\right] + \frac{Nt_1}{Nb_1}\left[\theta'' + \frac{\theta'}{(\eta+Rc)}\right] + \frac{RcLe_1}{2(\eta+Rc)}fg' - Le_1\lambda_\beta g\varphi^2 = 0, \tag{17}$$

$$\delta_1\left[\varphi'' + \frac{\varphi'}{(\eta+Rc)}\right] + \frac{Nt_1}{Nb_1}\left[\theta'' + \frac{\theta'}{(\eta+Rc)}\right] + \frac{RcLe_1}{2(\eta+Rc)}f\varphi' + Le_1\lambda_\beta g\varphi^2 = 0. \tag{18}$$

$$\theta(0) = 1,\ g'(0) = \lambda_\alpha g(0),\ \varphi'(0) = -\delta_1\lambda_\alpha\varphi(0),\quad \theta(\eta) = 0,\ g(\eta) = 0,\ \varphi(\eta) = 0,\ \eta \to \infty. \tag{19}$$

Where

$$Nt_1 = \frac{D_T(T_w-T_\infty)(\rho c)_p}{\nu_f T_\infty(\rho c)_f},\ Nb_1 = \frac{D_\beta c_\infty(\rho c)_f}{\nu_f(\rho c)_p},\ Le_1 = \frac{\nu_f}{D_\alpha},\quad \lambda_\beta = \frac{k_\lambda s c_\infty^2}{V_\infty},\ \lambda_\alpha = \frac{k_1\sqrt{\nu_f s/V_\infty}}{D_\alpha},\ \delta_1 = \frac{D_\beta}{D_\alpha},\ Pr = \frac{\mu_f c_p}{k_\gamma}. \tag{20}$$

The parameter Nt_1, Nb_1, Le_1, λ_β, λ_α, δ_1 and Pr are respectively the thermophoresis parameter, Brownian diffusion parameter, Lewis number, strength of homogenous reaction, strength of heterogeneous reaction, ratio of the diffusion coefficient and Prandtl number.

For case $\delta_1 = 1$, where the co-efficient D_α and D_β are equal, thus

$$g(\eta) + \varphi(\eta) = 1\,. \tag{21}$$

Thus, by using Eq. (21), Eqs. (17) and (18) along with boundary condition finally become

$$\left(g'' + \frac{g'}{(\eta+Rc)}\right) + \frac{Nt_1}{Nb_1}\left[\theta'' + \frac{\theta'}{(\eta+Rc)}\right] + \frac{RcLe_1}{2(\eta+Rc)}fg' - Le_1\lambda_\beta g(1-g)^2 = 0. \tag{22}$$

$$g'(0) = \lambda_\alpha g(0),\quad g(\infty) = 0. \tag{23}$$

3. Physical quantities for engineering interest

The physical quantities for engineering point of view are the skin friction coefficient, rate of mass and heat transfer which are given as

$$C_f = \frac{\overline{\tau}_{rs}^*}{V_\infty^2\rho_f},\quad Nu_s = \frac{s\overline{q}_w^*}{k_\gamma(T_w-T_\infty)},\quad Sh_s = \frac{s\overline{j}_w^*}{D_\beta C_\infty}. \tag{24}$$

Where $\overline{\tau}_{rs}^*$ represents the skin friction coefficient, $\overline{q}_w^*$ represent the rate of heat transfer and $\overline{j}_w^*$ indicates the mass flux along the surface i.e. in s-direction, which are given as

$$\overline{\tau}_{rs}^* = \mu_f\left[\frac{\partial w}{\partial r} - \frac{w}{r+R_0}\right]\Bigg|_{r=0},\quad \overline{q}_w^* = -k_\gamma\frac{\partial T}{\partial r}\Bigg|_{r=0},\quad \overline{j}_w^* = -D_\beta\frac{\partial C_\beta}{\partial r}\Bigg|_{r=0}. \tag{25}$$

By incorporating Eqs. (5), (15) and (25) in Eq. (24) we get

$$Re_s^{1/2}C_f = f''(0),\quad Re_s^{-1/2}Nu_s = -\theta'(0),\quad Re_s^{-1/2}Sh_s = -g'(0). \tag{26}$$

4. Modeling of entropy generation

After obtaining the fluid velocity and temperature and concentration fields we will used them to determine the entropy generation rate. The non-dimensional form for the volumetric flow rate of entropy generation for electrically conducting nanofluid with applied magnetic field and in presence of homogenous and heterogeneous chemical reactions is given by [38]

$$S_G = \overbrace{\frac{k_\gamma}{T_\infty^2}\left(\frac{\partial T}{\partial r}\right)^2}^{\text{Thermal Irreversibility}} + \overbrace{\frac{\mu}{T_\infty}\left[\frac{\partial w}{\partial r}+\frac{w}{r+R_0}\right]^2}^{\text{Irreversibility due to Fluid friction}} + \overbrace{\frac{\sigma M_o^2 (w-V_\infty)^2}{T_\infty}}^{\text{Irreversibility due to Joule heating}} + \overbrace{+\frac{D_\alpha}{C_\infty}\left(\frac{\partial C_\alpha}{\partial r}\right)^2+\frac{D_\alpha}{T_\infty}\left(\frac{\partial C_\alpha}{\partial r}.\frac{\partial T}{\partial r}\right)+\frac{D_\beta}{C_\infty}\left(\frac{\partial C_\beta}{\partial r}\right)^2+\frac{D_\beta}{T_\infty}\left(\frac{\partial C_\beta}{\partial r}.\frac{\partial T}{\partial r}\right)}^{\text{Mass diffusion irreversibility of homogeneous and hetrogeneous reactions}}, \quad (27)$$

Using Eqs. (5) and (15), the dimensionless form of Eq. (27) is given as

$$N_G = \gamma_1\theta'^2 + Brf'' + M_1 Br(f'-1)^2 + \frac{Brf'^2}{(\eta+Rc)^2} + \frac{2Brf'f''}{(\eta+Rc)} + \theta' g'(\beta_1-\beta_2) + \frac{g'^2}{\gamma_1}\left(\frac{\beta_1}{g}+\frac{\beta_2}{1-g}\right). \quad (28)$$

Bejan number can be expressed as follows

$$Be = \frac{\text{Heat and mass transfer irreversibility}}{\text{Total irreversibility}},$$

Or

$$Be = \frac{\gamma_1\theta'^2 + \theta' g'(\beta_1-\beta_2) + \frac{g'^2}{\gamma_1}\left(\frac{\beta_1}{g}+\frac{\beta_2}{1-g}\right)}{\gamma_1\theta'^2 + Brf'' + M_1 Br(f'-1)^2 + \frac{Brf'^2}{(\eta+Rc)^2} + \frac{2Brf'f''}{(\eta+Rc)} + \theta' g'(\beta_1-\beta_2) + \frac{g'^2}{\gamma_1}\left(\frac{\beta_1}{g}+\frac{\beta_2}{1-g}\right)}. \quad (29)$$

Where $\beta_1 = D_\alpha C_\infty / k_\gamma$ denotes the diffusion parameter regarding to homogeneous reaction and $\beta_2 = D_\beta C_\infty / k_\gamma$ denotes the diffusion parameter regarding to heterogeneous reaction, Brinkman number is denoted by $Br = \mu_f V_\infty^2 / k_\gamma (T_w - T_\infty)$ also the notation of temperature difference is $\gamma_1 = T_w - T_\infty / T_\infty$ and $N_G = \nu_f S_G T_\infty / k_\gamma V_\infty (T_w - T_\infty)$ represent entropy generation.

5. Discussions of result

In this section, we will discuss the physical features of the flow, heat and mass transfer for fluid velocity $f'(\eta)$, heat and mass transfer, $(\theta(\eta), g(\eta))$, entropy generation N_G and Bejan number Be through graphs 2–17. Furthermore, the magnitude of Nusselt number $Re_s^{-1/2}Nu_s$, Sherwood number $Re_s^{-1/2}Sh_s$ and skin friction coefficient $Re_s^{1/2}C_f$ are evaluated for different parameters through Tables 1–3. For this, we will solve the nonlinear boundary value problem consists of Eqs. (9), (16), (22), (28) and (29) with boundary conditions (8) and (9) numerically by shooting method incorporated by Runge-Kutta integrating scheme combined with Newton-Raphson method. Moreover, the validity of the obtained numerical results is also checked by a finite difference scheme called Keller-Box method and are found in good agreement.

Table 1
Numerical findings of $f''(0)$ for various values of M_1 and Rc.

M_1	Rc	$f''(0)$(shooting method)	$f''(0)$(Keller-Box method)
0.2	2	0.75408	0.75412
0.5		0.96618	0.96622
0.8		1.13753	1.13748
1.0		1.23772	1.23769
0.5	1.5	0.98270	0.98268
	3.0	0.93972	0.93967
	5.0	0.90209	0.90210
	7.0	0.87717	0.87719

5.1. For velocity

The pertinent aspects of magnetic parameter M_1 and curvature parameter Rc on velocity component $f'(\eta)$ are shown in Fig. 2 and 3. In Fig. 2 we observed that the momentum boundary thickness is reduced via the higher values of M_1. The physical arguments of this behaviour is that implementation of magnetic field alter the momentum boundary thickness for the lower magnetic Reynolds number. Moreover, Fig. 3 depicts that the velocity of the fluid rises via the higher values of Rc.

5.2. For transport phenomenon

In this subsection, we will discuss the effects of some pertinent parameters which include magnetic parameter M_1, Prandtl number Pr, radius of curvature Rc, thermophoresis parameter Nt_1, heat generation parameter α_1, Eckert number Ec, homogenous chemical reaction λ_β, Brownian motion parameter Nb_1, heterogeneous chemical reaction λ_α and Lewis number Le_1 on temperature distribution $\theta(\eta)$ and concentration distribution $g(\eta)$.

Table 2
Numerical values of $-\theta'(0)$ for different involved parameters, ()* represents the values obtained by shooting method and ()** represent the values are obtained by Keller-Box method by keeping $M_1 = 0.2, \lambda_\alpha = \lambda_\beta = 0.2$, $Pr = 1.5$ and $Le_1 = 0.1$ fixed.

Rc	Nb_1	Ec	Nt_1	α_1	$-\theta'(0)$
2	0.2	0.2	0.1	0.1	$(0.32089)^*, (0.32090)^{**}$
5					$(0.29377)^*, (0.29369)^{**}$
8					$(0.27962)^*, (0.27968)^{**}$
3	0.1				$(0.29857)^*, (0.29851)^{**}$
	0.5				$(0.34110)^*, (0.34110)^{**}$
	0.8				$(0.37427)^*, (0.37427)^{**}$
	0.2	0.5			$(0.25789)^*, (0.25785)^{**}$
		1.0			$(0.17251)^*, (0.17251)^{**}$
		1.5			$(0.08691)^*, (0.08687)^{**}$
		0.2	0.5		$(0.22465)^*, (0.22462)^{**}$
			0.8		$(0.17956)^*, (0.17950)^{**}$
			1.2		$(0.12868)^*, (0.12863)^{**}$
			0.1	0.05	$(0.40423)^*, (0.40418)^{**}$
				0.15	$(0.19469)^*, (0.19462)^{**}$
				0.2	$(0.05080)^*, (0.05075)^{**}$

Table 3
Numerical findings of $-g'(0)$ for various involved parameters, ()* represents the values obtained by shooting method and ()** represent the values are obtained by Keller-Box method by keeping $M_1 = 0.2, Rc = 3$, $Pr = 1.5$, $\alpha_1 = 0.1$ and $Ec = 0.2$ fixed.

λ_α	λ_β	Le_1	Nt_1	Nb_1	$-g'(0)$
0.2	0.2	0.5	0.1	0.1	−0.12705
0.5					−0.21257
0.8					−0.25588
0.2	0.5				−0.12273
	0.8				−0.11686
	1.2				−0.10376
	0.2	0.2			−0.12312
		0.6			−0.12822
		1.0			−0.13224
		0.5	0.3		−0.09279
			0.5		−0.03680
			0.6		−0.00435
			0.1	0.5	−0.13233
				0.8	−0.13369
				1.2	−0.13450

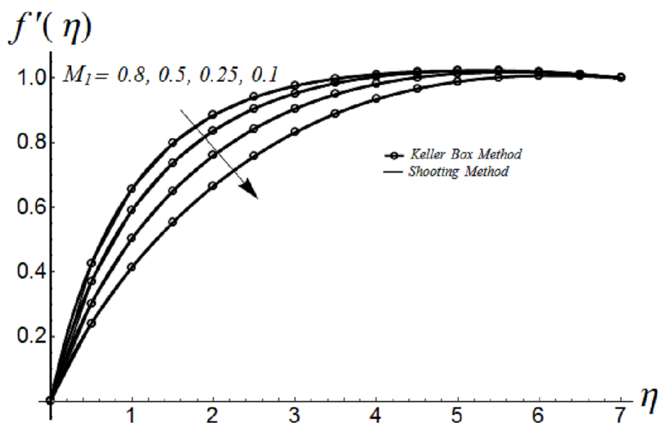

Fig. 2. Variation in $f'(\eta)$ via M_1 when $Rc = 1$.

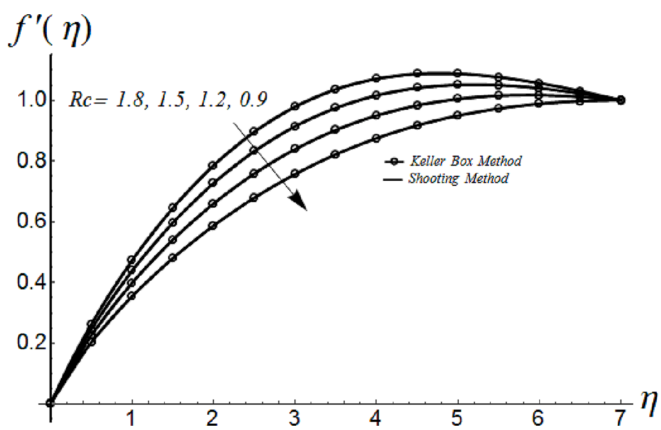

Fig. 3. Variation in $f'(\eta)$ via Rc when $M_1 = 0.05$.

Influence of Prandtl number Pr and magnetic parameter M_1 on temperature distribution $\theta(\eta)$ is shown in Fig. 4. It is observed that a decreasing behaviour exist for both the higher values Pr and M_1. The thickness of the thermal boundary layer also decreased in this case. The physical reasoning for this trend is that, the rate of thermal diffusion is reduced when parametric value of Pr is increased. The impacts of radius of curvature Rc and Brownian motion parameter Nb_1 on $\theta(\eta)$ is illustrated in Fig. 5. From this figure one can see that temperature and also the thickness of the thermal boundary layer of the fluid is decreased by uplifting the value of Rc and Nb_1. Fig. 6 shows the effects of heat generation parameter α_1 and Eckert number Ec on $\theta(\eta)$. As expected the temperature field rises via the higher values of α_1 and Ec. The variations of heterogeneous chemical reaction λ_α and thermophoresis parameter Nt_1 on $\theta(\eta)$ is shown in Fig. 7. Here we observed that advanced values of λ_α corresponds to decrease in $\theta(\eta)$. However, temperature of the fluid is increased correspond to higher values Nt_1, this is because Nt_1 is directly proportion to the coefficient of heat transfer rate which is associated to the hot fluid. Fig. 8 shows the influence of Lewis number Le_1 on $\theta(\eta)$. It is evident that $\theta(\eta)$ is reduced by increasing the value of Le_1.

Influence of Lewis number Le_1 and heterogeneous chemical reaction λ_α on concentration field $g(\eta)$ is displayed in Fig. 9. The concentration field $g(\eta)$ is increased when an increase in Le_1 occur, whilst it decreased via the larger values of λ_α. The impacts of radius of curvature Rc and thermophoresis parameter Nt_1 on $g(\eta)$ is shown in Fig. 10. It is noticed that the strength of concentration field is increased via larger values of Rc, though it is reduced by higher values of Nt_1. The influence of Brownian motion parameter Nb_1 and heat generation parameter α_1 on $g(\eta)$ is shown in Fig. 11. It is noticed that the strength of $g(\eta)$ is initially enhanced via the higher values of Nb_1, but after $\eta = 1.4$ it start decreasing. Also strength of $g(\eta)$ is decreased via the higher values of α_1, but after $\eta = 2.5$ it start increasing. The effects of homogenous chemical reaction λ_β and Eckert number Ec on concentration field $g(\eta)$ is displayed in Fig. 12. It is evident from this figure that concentration of the fluid is decreased by increasing both the parametric values of λ_β and Ec. Fig. 13 represents the influence of Prandtl number Pr and magnetic parameter M_1 on $g(\eta)$. It is noted from this figure that the $g(\eta)$ is reduced when an increase in Pr occur, however it is increased by increasing the value of M_1.

5.3. For entropy generation

In this subsection, we will examine the effects of some significant parameters like diffusion parameter regarding to homogeneous reaction β_1, diffusion parameter regarding to heterogeneous reaction β_2, Brinkman number Br, temperature difference γ_1, magnetic parameter M_1, thermophoresis parameter Nt_1, homogenous chemical reaction λ_β and heterogeneous chemical reaction λ_α on entropy generation N_G and Bejan number B_e.

The influence of diffusion parameter regarding to heterogeneous reaction β_2 and magnetic parameter M_1 on N_G and B_e is shown in Fig. 14 (a) and 14(b). It is noticed that, entropy generation N_G rises for higher values of M_1. This is because the larger values of M_1 generate further resistive force to the fluid motion which as a result enhances N_G. However, Bejan number B_e is reduced for higher values of M_1. Also, an increase in N_G and B_e are observed for higher values of β_2. The impacts of Brinkman number Br and diffusion parameter regarding to homogeneous reaction β_1 on N_G and B_e is displayed in Fig. 15(a) and 15(b). It is

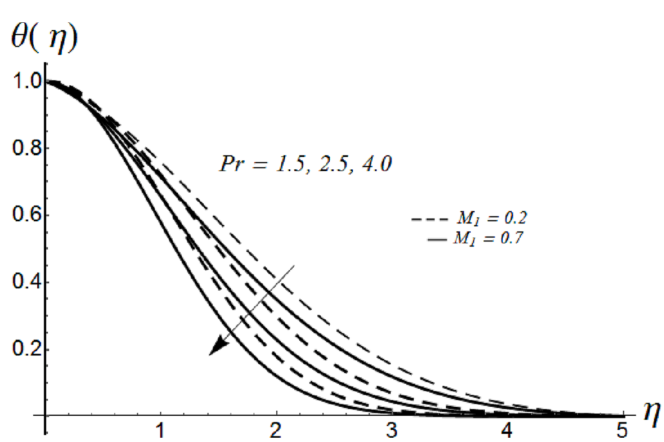

Fig. 4. Variation in $\theta(\eta)$ via M_1 and Pr when $Rc = 5$, $Nb_1 = 0.5$, $\alpha_1 = \lambda_\alpha = \lambda_\beta = Ec = 0.2$ $Nt_1 = 0.1$ and $Le_1 = 0.1$.

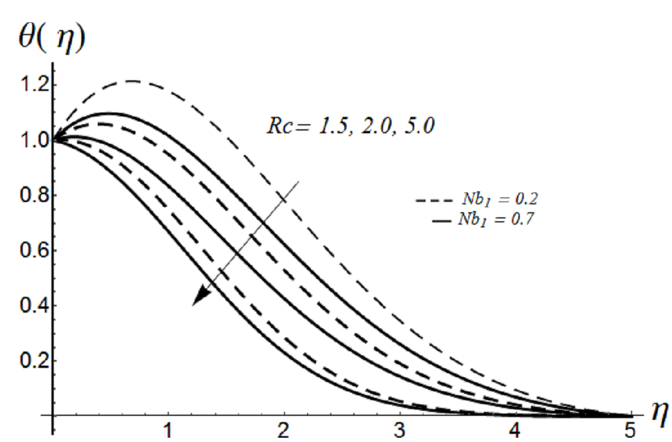

Fig. 5. Variation in $\theta(\eta)$ via Rc and Nb_1 when $M_1 = 0.2$, $Pr = 3$, $\alpha_1 = \lambda_\alpha = \lambda_\beta = Ec = 0.2$ $Nt_1 = 0.1$ and $Le_1 = 0.1$.

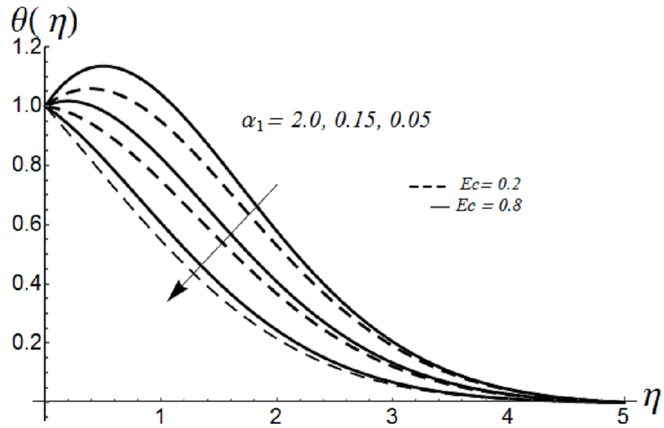

Fig. 6. Variation in $\theta(\eta)$ via α_1 and Ec when $M_1 = 0.2,\ Pr = 3,\ Rc = 2,\ Nb_1 = \lambda_\alpha = \lambda_\beta = 0.2\ Nt_1 = 0.1$ and $Le_1 = 0.1$.

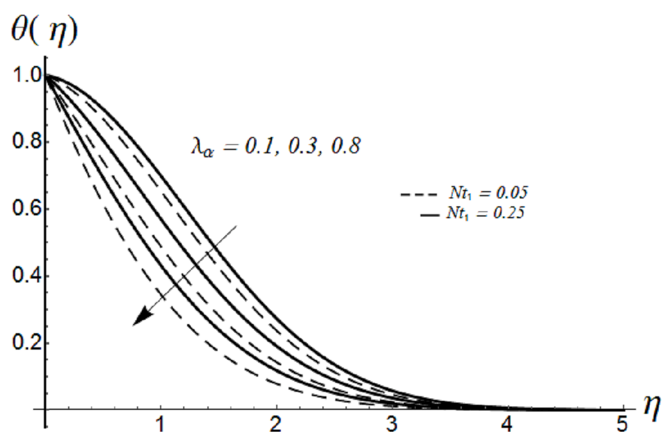

Fig. 7. Variation in $\theta(\eta)$ via λ_α and Nt_1 when $M_1 = 0.1,\ \alpha_1 = 0.2,\ Pr = 3,\ Rc = 5,\ Nb_1 = 1.5,\ Ec = 0.2,\ \lambda_\beta = 0.1$ and $Le_1 = 1$.

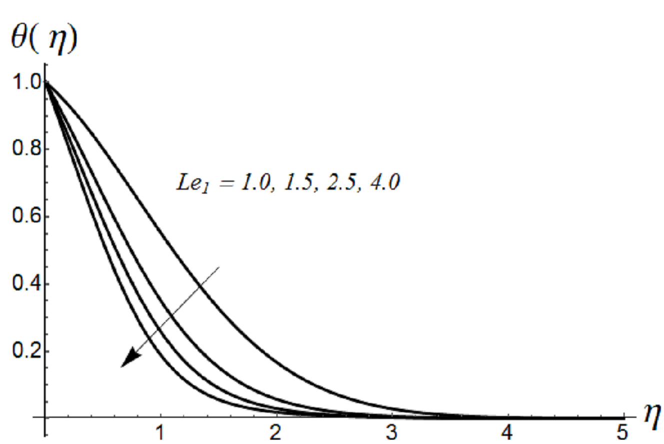

Fig. 8. Variation in $\theta(\eta)$ via Le_1 when $M_1 = 0.1,\ \alpha_1 = 0.2,\ Pr = 3,\ Rc = 5,\ Nb_1 = 1.5,\ Ec = 0.2,\ \lambda_\beta = 1,\ Nt_1 = 0.05$ and $\lambda_\alpha = 0.1$.

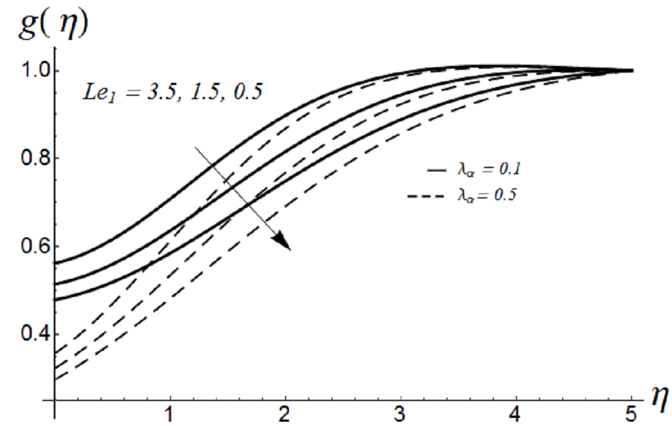

Fig. 9. Variation in $g(\eta)$ via Le_1 and λ_α when $M_1 = 0.1,\ \alpha_1 = 0.2,\ Pr = 2,\ Rc = 2,\ Nb_1 = 0.6,\ Ec = 0.1,\ \lambda_\beta = 0.3$ and $Nt_1 = 0.2$.

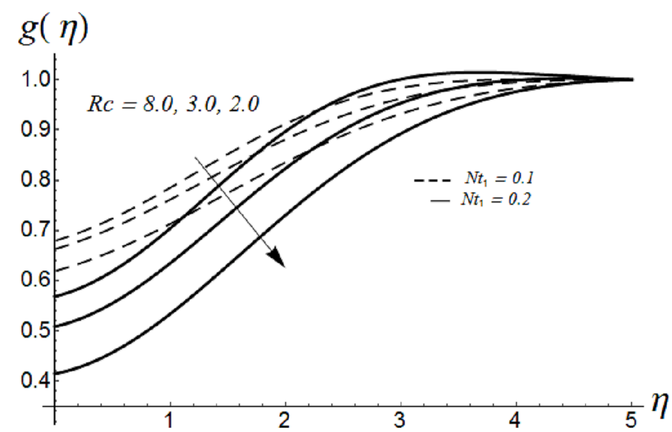

Fig. 10. Variation in $g(\eta)$ via Rc and Nt_1 when $M_1 = 0.1,\ \alpha_1 = 0.2,\ Pr = 2,\ Le_1 = 0.8,\ Nb_1 = 0.5,\ Ec = 0.1,\ \lambda_\beta = 0.3$ and $\lambda_\alpha = 0.1$.

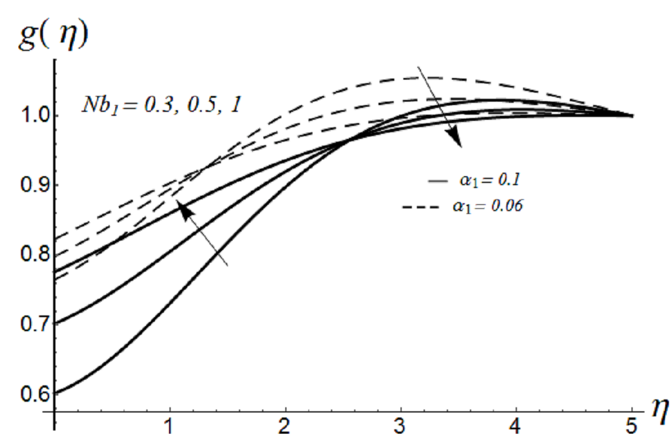

Fig. 11. Variation in $g(\eta)$ via Nb_1 and α_1 when $M_1 = 0.1,\ Nt_1 = 0.25,\ Pr = 2,\ Le_1 = 0.5,\ Rc = 2,\ Ec = 0.1,\ \lambda_\beta = 0.3$ and $\lambda_\alpha = 0.1$.

can be seen that, both entropy generation N_G and Bejan number B_e are decreased for higher values of β_1. However, N_G is increased for higher values β_1, whilst B_e decreases when an increment in β_1 occur. Fig. 16(a) and 16(b) is illustrated to see the influence of temperature difference γ_1 and thermophoresis parameter Nt_1 on N_G and B_e. It is noticed that both N_G and B_e are increased for higher values of γ_1. However, N_G and B_e are decreased for larger values Nt_1. Fig. 17(a) and 17(b) is made to see the effects of homogenous chemical reaction λ_β and heterogeneous chemical reaction λ_α on N_G and B_e. It is noticed that both N_G and B_e are reduced when an increment in λ_β occur. However, both N_G and B_e are increased for larger values λ_α.

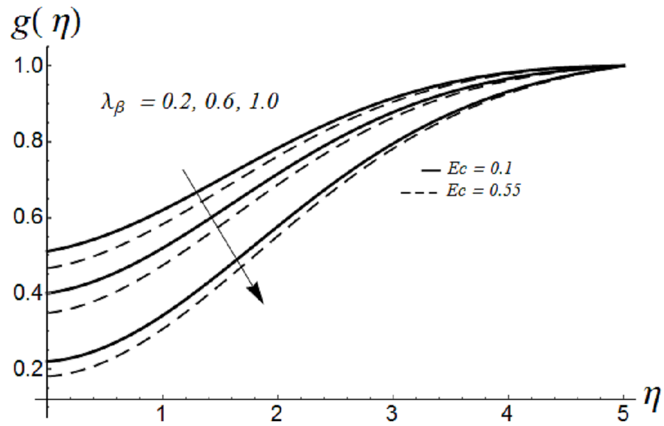

Fig. 12. Variation in $g(\eta)$ via λ_β and Ec when $M_1 = 0.1$, $Nt_1 = 0.2$, $Pr = 2$, $Le_1 = 0.8$, $Rc = 2$, $\alpha_1 = 0.1$, $Nb_1 = 0.6$ and $\lambda_\alpha = 0.1$.

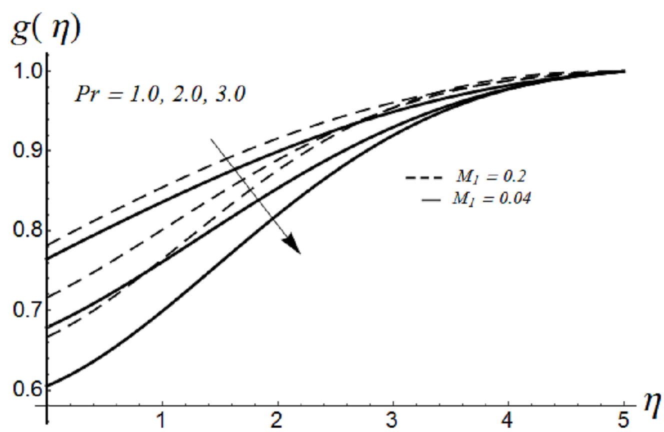

Fig. 13. Variation in $g(\eta)$ via M_1 and Pr when $\alpha_1 = 0.1$, $Nt_1 = 0.2$, $Nb_1 = 0.5$, $Le_1 = 0.8$, $Rc = 1$, $Ec = 0.05$, $\lambda_\beta = 0.3$ and $\lambda_\alpha = 0.1$.

5.4. For engineering interest

Significance of several pertinent parameters on skin friction coefficient $f''(0)$, Nusselt Number (rate of heat transfer) $-\theta'(0)$ and Schimdt number $-g(0)$ are numerically calculated in form of Tables 1-3. Moreover, the validity of the numerical results attained by the shooting method are also verified by a comparison with the numerical results obtained by a finite difference scheme called Keller-box method. The comparison of both the numerical results are found in good agreement.

5.4.1. Skin friction coefficient ($f''(0)$)

Table 1 is made to see the influence of magnetic parameter M_1 and curvature parameter Rc on skin friction coefficient $f''(0)$. It is evident from this table that absolute value of $f''(0)$ is increased via the higher values of M_1, whereas $f''(0)$ is decreased when an increment in Rc occur.

5.4.2. Nusselt number ($-\theta'(0)$)

Effects of Rc, Nt_1, Nb_1, α_1 and Ec on rate of Nusselt number $-\theta'(0)$ are shown in Table 2. It is observed that rate of heat transfer is decreased by increasing the values of Rc, Nt_1, α_1 and Ec, whereas it increases for Nb_1.

5.4.3. Schmidt number ($-g(0)$)

Impacts of λ_α, λ_β, Nb_1, Le_1 and Nt_1 on Schimdt number $-g(0)$ are shown in Table 3. It is noticed that rate of mass transfer is decreased by increasing the values of λ_β and Nt_1, however it increases for λ_α and Nb_1.

6. Conclusions

The main objective of the current study is to present a meaningful investigation for the Blasius flow, heat and mass transfer in a nanofluid past a curved surface. The impacts of Joule heating and heat generation is also considered in the energy equation. Furthermore, effects of homogenous and heterogeneous chemical reactions are also taken in the nanoparticle concentration equation. The optimization of energy is also carried out by taking entropy generation method. Numerical solution is attained for the governing flow equations.

The main finding of the current study are as follows:

- The fluid velocity $f'(\eta)$ is enhanced with radius of curvature Rc. However, it is reduces with an increments in magnetic parameter M_1.
- The temperature distribution $\theta(\eta)$ rises through an increments in the parameters α_1, Ec and Nt_1. While it shows opposite behavior for higher estimations of Pr, Rc, Ec, M_1, Nb_1, Le_1 and λ_α.
- The concentration distribution $g(\eta)$ is decreased against larger values of Pr, Ec, Nt_1, Le_1, λ_α, λ_β and α_1, however for growing values of Rc, M_1, Nb_1 and Le_1 $g(\eta)$ is enhanced.
- The entropy generation N_G is increased for higher estimations of β_2, M_1, Br, γ_1, λ_α and λ_β. though, it reduces when increment in β_1 and Nt_1 occur.
- The Bejan number Be reduces for higher estimations of β_1, M_1, Br, λ_β and Nt_1, though it rises for higher values of β_2, γ_1 and λ_α.
- Skin friction coefficient $f''(0)$ enhanced for higher values of M_1, whilst it decreases with higher estimations of Rc.
- Nusselt number $-\theta'(0)$ is reduced for developed values of Rc, Ec, Nt_1 and α_1, whilst it increases with higher estimations of Nb_1.
- Schmidt number $-g(0)$ is enhanced for higher values of λ_α, Le_1 and Nb_1, however it decreases with larger values of λ_β and Nt_1.

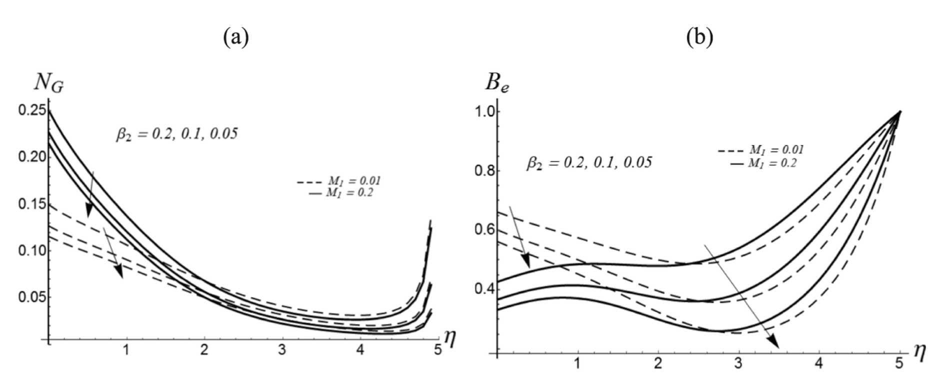

Fig. 14. Variation in N_G and Be via M_1 and β_2 when $\alpha_1 = 0.05$, $Nt_1 = 0.01$, $Ec = 0.1$, $\lambda_\beta = 0.1$,$Nb_1 = 0.3$, $Le_1 = 0.3$, $Rc = 2$, $\gamma_1 = 0.2$, $\beta_1 = 0.3$, $\lambda_\alpha = 0.1$, $Pr = 3$ and $Br = 0.2$.

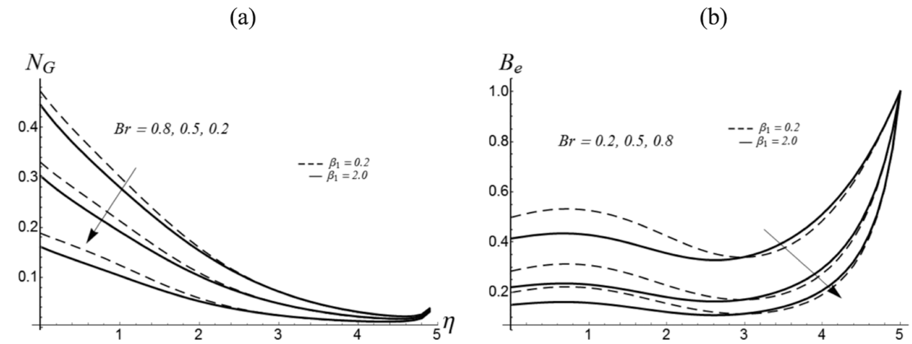

Fig. 15. Variation in N_G and Be via Br and β_1 when $\alpha_1 = 0.05$, $Nt_1 = 0.01$, $Le_1 = 0.5$, $Rc = 2.5$, $Nb_1 = 0.2$, $Ec = 0.1$, $\lambda_\beta = 0.2$, $\gamma_1 = 0.3$, $\beta_2 = 0.1$, $\lambda_\alpha = 0.1$, $Pr = 3$ and $M_1 = 0.1$.

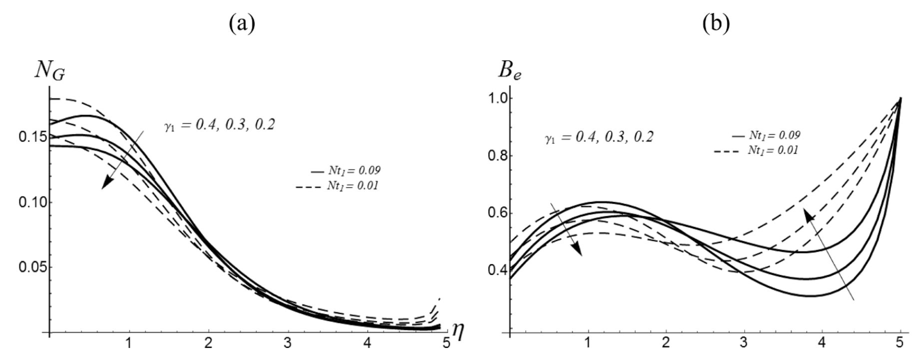

Fig. 16. Variation in N_G and Be via γ_1 and Nt_1 when $\beta_1 = 0.2$, $\alpha_1 = 0.1$, $Le_1 = 1$, $Br = 0.2$, $Nb_1 = 1.0$, $Ec = 0.2$, $\lambda_\beta = 0.1$, $Rc = 4$, $\beta_2 = 0.1$, $\lambda_\alpha = 0.1$, $Pr = 3$ and $M_1 = 0.1$.

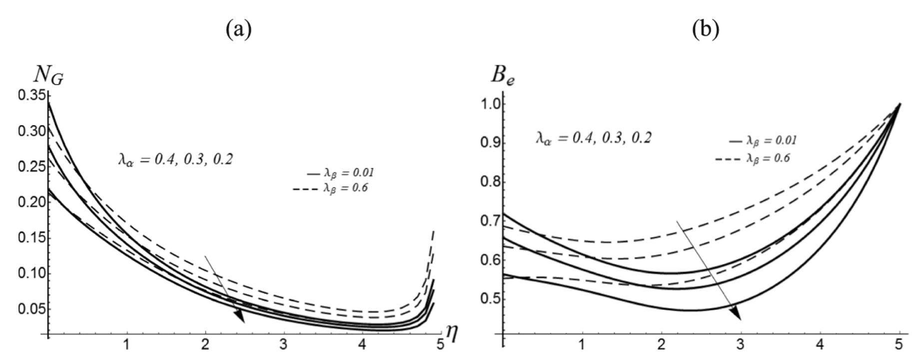

Fig. 17. Variation in N_G and Be via λ_α and λ_β when $\beta_1 = 0.2$, $\alpha_1 = 0.1$, $Le_1 = 1$, $Br = 0.2$, $Nb_1 = 1.0$, $Ec = 0.1$, $Nt_1 = 0.01$, $Rc = 2$, $\beta_2 = 0.1$, $\gamma_1 = 0.2$, $Pr = 3$ and $M_1 = 0.1$.

CRediT authorship contribution statement

M. Naveed: Conceptualization, Data curation, Investigation, Formal analysis, Methodology, Writing – original draft.

Declaration of Competing Interest

The authors declare that they have no known competing financial interests or personal relationships that could have appeared to influence the work reported in this paper.

Data availability

Data will be made available on request.

Acknowledgment

I am thankful to the worthy reviewers for their encouraging comments and productive suggestions to increase the quality of the manuscript.

References

[1] M.V. Karwe, Y. Jaluria, Numerical simulation of thermal transport associated with a continuous moving flat sheet in materials processing, ASME Heat Transfer 113 (1991) 612–619.
[2] H. Blasius, Grenzschicten in Flussigkeitenmitkleinerreibung, Z. Math. Phys. 56 (1908) 1–37.
[3] A. Pantokratoras, T. Fang, Blasius flow with nonlinear thermal radiation, Meccanica 49 (6) (2014) 1539–1545.
[4] M. Naveed, Z. Abbas, M. Sajid, Nonlinear radiative heat transfer in Blasius and sakiadis flows over a curved surface, Int. J. Thermophys. (2017) 38:14.
[5] S.P.A. Devi, P. Suriyakumar, Effect of magnetic field on Blasius and Sakiadis flow of nanofluid past an inclined plate, J. Taibah Uni. Sci. 11 (2017) 1275–1288.

[6] R.C. Bataller, Numerical comparison of Blasius and Sakiadis flows, Mathematika 26 (2) (2010) 187–196.

[7] P.O. Olanrewaju, J.A. Gbadeyan, O.O. Agboola, S.O. Abah, Radiation and viscous dissipation effects for the Blasius and Sakiadis flows with a convective surface boundary condition, Int. J. Adv. Sci. Technol. 2 (4) (2011) 102–115.

[8] S. Sadeqi, N. Khabazi, K. Sadeghy, Blasius flow of thixotropic fluids, A numerical study, Commun. Nonliner Sci. Numer. Simul. 16 (2011) 711–721.

[9] Z. Lu, C.K. Law, An iterative solution of the Blasius flow with surface gasification, Int. J. Heat Mass Transfer 69 (2014) 223–229.

[10] A. Pantokratoras, Blasius and Sakiadis flow with suction and non-linear Rosseland thermal radiation, Int. J. Thermofluids 10 (2021), 100067.

[11] S. U. S. Choi, Enhancing thermal conductivity of fluids with nanoparticles, in The Proceeding of the 1995 ASME International Mechanical Engineering Congress and Exposition, San Francisco, USA, ASME, FED 231/MD 66(1995)99-105.

[12] J. Buongiorno, Convective transport in nanofluid, J. Heat Transfer 128 (2006) 240–250.

[13] M. Naveed, Z. Abbas, M. Sajid, Thermophoresis and Brownian effects on the Blasius flow of a nanofluid due to a curved surface with thermal radiation, Eur. Phys. J. Plus 131 (2016) 214.

[14] N.V. Ganesh, Q.M. Al-Mdallal, K. Reena, S. Aman, Blasius and Sakadis slip flow of nanofluid with different geometry of boehmite alumina nanoparticles, Case Studies Therm. Sci. 16 (2019), 100546.

[15] R. Kumar, R. Kumar, K. Vajravelu, M. Sheikholeslami, Three-dimensional stagnation flow of Casson nanofluid through Darcy-Forechheimer space: A reduction to Blasius/Sakiadis flow, Chin. J. Phys. 68 (2020) 874–885.

[16] Z. Abbas, M. Naveed, R. Tabassum, I. Ahmad, Influence of Hall and Joule heating on a magnetic nanofluid (Fe3O4) flow on a rotating disk with generalized slip condition, Heat Transf. 50 (7) (2021) 7271–7290.

[17] M.J. Uddin, W.A. Khan, F.T. Zohra, A.M. Ismail, Blasius and Sakiadis slip flows of nanofluid with radiation effects, J. Aerosp. Eng. 29 (4) (2015) 04015080.

[18] M. Imran, Z. Abbas, M. Naveed, N. Salamat, Impact of Joule heating and melting on time-dependent flow of nanoparticles due to an oscillatory stretchable curved wall, Alex. Eng. J. 60 (4) (2021) 4097–4113.

[19] S. Ahmad, A.M. Rohni, I. Pop, Blasius and Sakiadis problems in nanofluids, Acta Mech. 218 (3–4) (2011) 195–204.

[20] M. Naveed, S. Ali, J. Hasnain, Z. Abbas, Analysis of the effect of joule heating and hall current on flow of hybrid nanofluid over a curved stretching surface with melting boundary condition, Heat Trans. Res. 52 (5) (2021) 1–16.

[21] W.A. Khan, R. Culham, O.D. Makinde, Hydromagentic Blasius flow of power law nanofluid over a convectively heated vertical plate, Cand. J. Chem. Eng. 93 (2015) 1830–1837.

[22] P.M. Krishna, R.P. Sharma, N. Sandeep, Boundary layer analysis of persistent moving horizontal needle in Blasius and Sakiadis magnetohydrodynamic radiative nanofluid flows, Nucl. Eng. Technol. 48 (8) (2017) 1654–1659.

[23] M. Imran, M. Naveed, B. Iftikhar, Z. Abbas, Heat transfer analysis in a curvilinear flow of hybrid nanoliquid across a curved oscillatory stretched surface with nonlinear thermal radiation, ZAMM-J, Appl. Mathe. Mech./Zeit. Ange. Mathe. Mecha. (2023) e202200600.

[24] M.M. Bhatti, K. Al-Khaled, S.U. Khan, W. Chammam, M. Awais, Darcy-Forchheimer higher-order slip flow of Eyring-Powell nanofluid with nonlinear thermal radiation and bioconvection phenomenon, J. Disp. Sci. Tech. 44 (2) (2023) 225–235.

[25] A.T. Olatundun, O.D. Makinde, Analysis of Blasius flow of hybrid nanofluid over a convectively heated surface, Defect Diffusion, Forum 377 (2017) 29–41.

[26] Z. Abbas, S. Hussain, M. Naveed, A. Nadeem, A. Ali, Analysis of joule heating and generalized slip flow in ferromagnetic nanoparticles in a curved channel using Cattaneo-Christov heat flux theory, Therm. Sci. 26 (1 Part B) (2022) 437–448.

[27] M. Sajid, S.A. Iqbal, M. Naveed, Z. Abbas, Effect of homogeneous and heterogenous reactions on magentohydrodynamics flow of nanofluid for the Blasius flow with thermal radiation, J. Molec. Liq. 233 (2017) 115–121.

[28] Z. Abbas, M. Imran, M. Naveed, Impact of equally diffusive chemical reaction on time dependent flow of Casson nanofluid due to oscillatory curved stretching surface with thermal radiation, Arab J Sci Eng 47 (12) (2022) 16059–16078.

[29] A.A. Opanuga, O.O. Agboola, H.I. Okagbue, P.O. Ogunniyi, Influence of inclined magnetic field and chemical reaction on the entropy generation of Blasius and Sakiadis flow, Sci. Afr. 10 (2020) e00640.

[30] L. Ali, B. Ali, X. Liu, S. Ahmed, M.A. Shah, Analysis of bio-convective MHD Blasius and Sakiadis flow with Cattaneo-Christov heat flux model and chemical reaction, Chi. J. Phys. 77 (2022) 196–1975.

[31] M. Naveed, M. Awais, Z. Abbas, M. Sajid, Analysis of Joule heating in a chemically reactive flow of time dependent Carreau-nanofluid over an axisymmetric radially stretched sheet using Cattaneo-Christov heat flux model, Ricer, Mate. (2021) 1–18.

[32] S.M. Tausif, K. Das, P.K. Kundu, Modified homogeneous and heterogeneous chemical reaction and flow performance of maxwell nanofluid with Cattaneo-Christov heat flux law, J. Engi. Thermophys. 31 (1) (2022) 64–77.

[33] M. Naveed, M. Imran, S. Akhtar, Z. Abbas, S. Ullah, Dynamics of melting heat transfer in thermally developed and chemically reactive flow of Eyring-Powell liquid through a curved channel, Ricer. Mater. 72 (1) (2023) 299–316.

[34] N.S. Khan, U.W. Humphries, W. Kumam, P. Kumam, T. Muhammad, Bioconvection Casson nanoliquid film sprayed on a stretching cylinder in the portfolio of homogeneous-heterogeneous chemical reactions, ZAMM-J, Appl. Math. Mech./ Zeits. Ange. Math. Mech. 102 (5) (2022) e202000222.

[35] M. Naveed, M. Imran, and S. Gul, Heat transfer analysis in hydromagnetic flow of couple stress fluid in presence of homogeneous and heterogeneous chemical reactions over a porous oscillatory stretchable sheet, Adv. Mech. Engi. 15(2), (2023) 16878132231155823.

[36] M.I. Afidi, M. Qasim, Second law analysis of Blasius flow with nonlinear Rosseland thermal radiation in the presence of viscous dissipation, Prop. Power Resse. 8 (3) (2019) 234–242.

[37] Z. Abbas, M. Naveed, M. Hussain, N. Salamat, Analysis of entropy generation for MHD flow of viscous fluid embedded in a vertical porous channel with thermal radiation, Alex. Eng. J. 59 (2020) 3395–3405.

[38] M.I. Khan, S.A. Khan, T. Hayat, S. Qayyum, A. Alsaedi, Entropy generation analysis in MHD flow of viscous fluid by a curved stretching surface with cubic autocatalysis chemical reaction, Eur. Phys. J. Plus 135 (2020) 249.

[39] M. Khan, T. Salahuddin, M. Altanji, A viscous dissipated Blasius boundary layer flow with variable thermo-physical properties: An entropy generation study, Int. Commun. Heat Mass Transf. 131 (2022), 105873.

[40] F. Shah, S.A. Khan, K. Al-Khaled, M.I. Khan, S.U. Khan, N.A. Shah, R. Ali, Impact of entropy optimized Darcy-Forchheimer flow in MnZnFe2O4 and NiZnFe2O4 hybrid nanofluid towards a curved surface, ZAMM-J. Appl. Mathe. Mech. Zeit. Ange. Mathe. Mech. 102 (3) (2022) e202100194.

[41] A. Abbasi, K. Al-Khaled, F. Zouidi, S.U. Khan, M.I. Khan, O.T. Bafakeeh, W. Farooq, R. Choudhari, Blood-based electro-osmotic flow of non-Newtonian nanofluid (Carreau-Yasuda) in a tapered channel with entropy generation, ZAMM-J. Appl. Mathe. Mech. Zeit. Ange. Mathe. Mech. 103 (5) (2023) e202100351.

[42] W. Aich, K. Javid, K. Al-Khaled, K. Gachem, D. Khan, S.U. Khan, L. Kolsi, The ciliated flow of water-based graphene oxide and copper nanoparticles (GO-Cu/ H2O) in a complex permeable tube with entropy generation phenomenon, Waves Rand. Compl. Med. (2022) 1–17.

[43] M. Naveed, M. Imran, Z. Abbas, A. Nadeem, Analysis of entropy generation and Joule heating on curvilinear flow of thermally radiative viscous fluid due to an oscillation of curved Riga surface, Int. J. Mod. Phys. C. 33 (07) (2022) 2250087.

[44] N. Khan, I. Riaz, M.S. Hashmi, S.A. Musmar, S.U. Khan, Z. Abdelmalek, I. Tlili, Aspects of chemical entropy generation in flow of Casson nanofluid between radiative stretching disks, Entropy 22 (5) (2020) 495.